Local energy exchange in a storage-ring free-electron laser

G. De Ninno,[1,2] M. E. Couprie,[1,2] D. Nutarelli,[1,2] D. Garzella,[1,2] E. Renault,[1,2] and M. Billardon[2,3]
[1]*CEA/DSM/DRECAM, Gif sur Yvette, France*
[2]*LURE, Orsay, France*
[3]*ESPCI, Paris, France*
(Received 15 December 2000; published 17 July 2001)

In this paper a theoretical model is presented, which is based on a pass to pass analysis of the localized interaction between a short laser pulse with a wider electron distribution. It can be applied to a large class of physical phenomena and, in particular, to the case of a storage-ring free-electron laser (FEL). Numerical results are confirmed by experimental measurements done on the ACO and Super-ACO FELs.

DOI: 10.1103/PhysRevE.64.026502 PACS number(s): 41.60.Cr, 29.20.Dh

I. INTRODUCTION

The interaction between a coherent light source and a relativistic electron beam can lead to various physical phenomena, such as Compton backscattering [1], femtosecond x-rays production [2], electron acceleration [3] and free-electron lasers (FELs).

After the first operation of a FEL in the infrared spectral range on a linear accelerator in 1977 [4], a second FEL was installed on the ACO storage ring and provided the first visible radiation in 1983 [5]. Present storage-ring based FELs still supply the shortest FEL wavelength in the oscillator configuration on DUKE [6] and in the harmonic generation scheme in Super-ACO ring [7]. Recent studies of the storage-ring FEL dynamics led to a deeper understanding of the role played by some complex beam characteristics (microwave [8] and head-tail instabilities [9], potential well distortion [10,11] coherent synchrotron oscillations [12], variable momentum compaction operation [13]) on the laser performances. Besides feedback systems implemented on different machines allowed to reach a high level of stability of the source [14]. User applications performed since 1993 on the Super-ACO FEL have demonstrated a very good quality offered by such sources in terms of tuneability, high average power, rather short pulse duration, and high degree of coherence [15]. These characteristics make, for example, the FEL very suitable for two colors experiments performed in combination with the naturally synchronized synchrotron radiation [16]. Considering such a stage of maturity, new perspectives are opened by future operation of FEL facilities such as DUKE [6] and ELETTRA [17] or of new synchrotron radiation centres such as SOLEIL [18].

A storage-ring FEL is a coherent and tuneable radiation source generated by the energy exchange between a relativistic electron beam and an electromagnetic wave stored in an optical cavity. The light pulses interact many times with the same electron bunch. As a consequence the beam longitudinal distributions are modified and a saturation mechanism may be induced leading to the laser equilibrium. Storage-ring FELs have a complex dynamics because the laser pulse does not interact with a fresh electron bunch (as it happens for LINAC based FELs). The laser performances tightly depend on the evolution of the beam parameters (such as electron density, energy, and temporal distributions).

Classical approaches to the study of the evolution of the FEL-beam system [19,20] are based on a certain number of assumptions. First, only the steady-state regime is considered: the equilibrium is assumed to be always reached after a disregarded transient regime. Second, the interaction between the bunch and the FEL pulse is assumed to take place homogeneously over the whole electron distribution (in a way that does not take into account the different size of the electron bunch and the FEL pulse). Moreover, the well-known super modes approach [21] evaluates the FEL induced heating of the longitudinal distributions of the electron bunch in terms of a modification of their rms values. This means that the distributions are assumed to maintain a Gaussian shape (that is the natural solution of the Fokker-Plank equation when the FEL is absent) once the steady-state is attained.

A more realistic approach has been more recently proposed [22,23]. Theoretical simulations done by making use of the model detailed in [22] allow one to follow the evolution of the electron distribution in the beam longitudinal phase space during the FEL-beam interaction. In fact, the analysis shows that the temporal beam distribution does not maintain a Gaussian shape but it is instead significantly modified during the FEL on set. The origin of this phenomenon can be traced back to the different size of the electron distribution and the laser pulse (the latter being much shorter): the FEL creates a local hot spot where electron diffusion is maximum. Synchrotron oscillations move electrons into the hot spot where they interact with the optical pulse, amplify it and diffuse. As a consequence, the electron beam energy spread grows everywhere, the system gain decreases, and the FEL reaches the saturation.

The theoretical model that is proposed here takes a step further. First of all, it includes the interaction between the electron beam and the storage-ring environment (which is missed in the previous model). The effect of the electron beam instabilities generated by the wake fields on the FEL evolution has been the subject of various investigations [24–27]. Nowadays there is a general agreement on the fact that longitudinal instabilities and FEL are strongly correlated (generally competing) mechanisms generating noise that manifests in an increase of the beam energy spread. A correct modelization of the FEL-beam interaction has, therefore,

to include the effect of the wake fields on the electron beam and on the FEL evolution.

Moreover, for the first time, to the best of our knowledge, a pass to pass analysis of the FEL-beam interaction is supported by a fully satisfactory agreement with experimental measurements. The case of the ACO and the Super-ACO FELs (operated in different regimes) is considered.

Finally, the model proposed in this paper can also be generally applied to the interaction of a relativistic electron beam with an external laser. In this case, a careful pass to pass analysis may, for example, provide important informations about the maximum interaction rate allowing an adequate regeneration of the electron distributions. In the following, the attention will be mostly concentrated on the interaction during the transient regime. A number of experimental observations show that the system does not necessarily reach a steady state: chaotic regimes of the laser intensity have been observed for the case of the ACO and the Super-ACO FELs [28]; limit cycle regimes appear for a small detuning (leading to a macrotemporal pulse structure at the millisecond scale) on the Super-ACO [29] and UVSOR [30] FELs. Moreover, even if the steady state is reached, small perturbations of the optics (as, for example, the unavoidable heating of the cavity mirrors) or of the beam stability may lead the system out of equilibrium (that is again in a transient regime). Finally, the *Q*-switched operation mode (during which the system never attains the steady state) is commonly used for certain FEL applications to enhance the laser power.

The model is presented in Sec. II. In Sec. III the FEL action on the beam longitudinal distributions is investigated. The case of the FEL that will be installed on SOLEIL is used as a general example of the implications of the proposed model (Sec. III A). In Sec. III B the analysis is extended to all the storage-ring FELs presently in activity. Section III C contains a comparison between the theoretical simulations and measurements performed on the Super-ACO (operated in *Q*-switched regime) and the ACO (operated in cw regime) FELs. In Sec. IV the effect of the localized interaction on the electron density, on the modulation rate (i.e., the ''contrast'' of the interference fringes of the optical klystron spectrum) and, as a consequence, on the FEL gain is analyzed for the case of the Super-ACO. The definition of a local gain can be used to partially explain the difference between theoretical and measured laser rise time observed on the Super-ACO FEL.

II. THE MODEL

A case of a storage-ring FEL implemented on an optical klystron (consisting of two undulators separated by a dispersive section, creating a large wiggle of magnetic field [31,33]) is considered. Since the proper laser mode of the optical cavity is established after several hundred light paths, the longitudinal and transverse laser dynamics are assumed to be decoupled. Electron dynamics in the longitudinal phase space is treated by using a pass to pass model [34] (distributions are statistically determined):

$$\tau_{n+1} = \tau_n - \alpha T_0 \epsilon_n , \tag{1}$$

$$\begin{aligned}\epsilon_{n+1} = \epsilon_n + eV_{\mathrm{rf}}/E_0 \sin(\omega_{\mathrm{rf}}\tau_{n+1} + \phi) - U_{\mathrm{rad}}/E_0 - \mathcal{D}(\epsilon_n, \tau_n) \\ + \mathcal{R}(\epsilon_n, \tau_n) - \mathcal{A}(\tau_n) + B\sqrt{I(\tau_n)}\sin(\omega_{\mathrm{las}}\tau_n + \psi) \\ - PI(\tau_n)\cos[4\pi(N + N_d)\epsilon_n].\end{aligned} \tag{2}$$

where τ_n is the relative position of the electron at pass n with respect to the synchronous electron, ϵ_n its relative normalized energy, ω_{rf} and V_{rf} the pulsation and the voltage of the main rf cavity with associate phase ϕ, α the momentum compaction factor, e is the electron charge, E_0 the nominal electron energy, U_{rad} the energy radiated by synchrotron radiation, $D(\epsilon_n, \tau_n)$ the synchrotron damping term, $R(\epsilon_n, \tau_n)$ is associated with the stochastic process of photon emission. The FEL is characterized by the optical pulsation ω_{las}, the relative phase ψ and the intensity I. The amplification of only one single wavelength is here considered. In fact simulations are started just after the beginning of the laser growth and this justifies the previous hypothesis. A more accurate analysis of the laser spectral evolution has been carried out in [35]. The normalized FEL distribution for the FEL pulse at the center of the electron distribution $I(\tau_n) = I_0 \exp(-\tau_n^2/2\sigma_{\mathrm{las}}^2)$ has a smaller rms width σ_{las} than the electronic distribution. The effect of the interaction of the electron beam with the ring environment is taken into account by the term $r(\tau_n)$ which includes an resistance capacity inductance (RCL) model of the machine impedance. In particular, a good agreement with measurements presented in Sec. III C has been obtained by modeling the wake field by means of a simple exponential corresponding to a first-order longitudinal coupling impedance ($C=0$) [32]. The last two terms modelize the FEL interaction. $B\sqrt{I(\tau_n)}\sin(\omega_{\mathrm{las}}\tau_n + \psi)$ corresponds to the FEL induced microbunching on the electron bunch, where the bunching factor B depends on the FEL intensity. The bunching takes place for the electrons that overlap with the FEL Gaussian distribution. Because of the synchrotron motion, different electrons see the FEL localized distribution at different passes. The last term $-PI(\tau_n)\cos[4\pi(N + N_d)\epsilon_n]$ represents the energy loss by laser radiation, P being the FEL power, N the number of period of the undulator, N_d is the interference order due to the dispersive section of the optical klystron [33]. The laser light quantum emission is neglected.

This model naturally applies to an FEL system but it can also be used to study the interplay between a relativistic electron bunch and an external laser in view, for example, of generating femtosecond x-ray pulses [2].

III. FEL ACTION ON THE ELECTRON BUNCH

The model presented in the preceding section can be applied to the study of laser action on the longitudinal form of the electron bunch. The case of all the storage-ring FELs presently in activity will be analyzed.

The general consequences of the localized character of the laser-beam interaction on the longitudinal beam distributions will be illustrated by considering the case of the FEL that will be installed on SOLEIL. In Sec. III A the numerical simulations based on the model presented in Sec. II and performed for the SOLEIL FEL are reported. Similar results

TABLE I. Characteristics of different storage ring FELs.

	SOLEIL	ELETTRA	S.ACO	DUKE	UVSOR	ACO
Beam energy (MeV)	1500	1000	800	1000	500	240
Bunch width (ps)	25	85	95	60	95	100-1000
Rms FEL width (ps)	2-6	9	20	1.4-26	7	2-6
Spectral range (nm)	400-150	350-220	vis.-300	193.7-730	vis.-238	650-460
Pulse period (ns)	280	864	120	358.5	178	37
FEL gain (%)	10-50	30	3	15	3	0.6

hold for the Super-ACO, ACO, ELETTRA, DUKE and UV-SOR FELs (see Sec. III B). In Sec. III C good agreement is shown between theoretical results and measurements for the case of the Super-ACO and the ACO FELs.

In Table I are reported the characteristics of different storage-ring FELs that are relevant for the present analysis.

A. Numerical results for the case of the SOLEIL FEL

The enhancement of the laser peak power of the SOLEIL FEL operated in *Q*-switch mode is shown in Fig. 1(a). Figure 1(b) shows the rms bunch lengthening of the temporal distribution related to the increase of the energy spread produced by the interaction. After an initial heating during the rise time of the FEL pulse, the energy spread slowly reaches a constant regime with superimposed coherent synchrotron oscillations. These oscillations are more evident if the behavior of the center of mass of the bunch τ_0 is considered [Fig. 1(c)]. Electrons located at the center of the distribution (where the interaction takes place) start to perform large oscillations from the head to the tail of the bunch as the FEL macropulse decreases. The enhancement of the oscillations accomplished by the barycenters of the longitudinal distributions is shown in Fig. 2. The temporal distribution does not maintain the initial Gaussian form (FEL off) as it is clearly demonstrated by the change of its third order momentum *k* [Fig. 1(d)]. Figure 1(e) shows the gain decrease due to the FEL saturation. The perturbation changes the amplitude of the synchrotron oscillations. The reorganization of the bunch population is shown in Fig. 3. During the FEL rise time (that is, between 50 and 90 μs), the phase coordinates of the electrons are strongly perturbed (especially the relative energy ϵ). At the end of the laser macropulse (that is, after about 200 μs) synchrotron oscillations become regular again but their amplitude is enhanced. If the laser is not started again, the amplitude of the oscillations is dumped in a period of the order of (few times) the synchrotron damping time (about 20 ms for the case of SOLEIL).

The evolution of the temporal and energy distributions is presented in Fig. 4. The FEL micropulse is centered with respect to the temporal beam distribution (perfect tuning condition). The initial distributions (curve *a*, FEL off) are Gaussian; when the FEL macropulse grows (curve *b*) a deformation starts to become evident and during the macropulse decrease (curve *c*) the temporal distribution narrows in its center and a hole appears. The presence of a hole burning in the energy distributions can be stressed by representing only the electrons located at the FEL pulse position [Fig. 4(c)]. The hole is the signature of the localized interaction and is generated by the fact that the electrons located around the center of the distributions interact on average for a longer time with the FEL than the electrons at the edge, thus providing more energy to the FEL. During the last part of the FEL macropulse (curves *d* to *i*) the electrons start to diffuse, the distributions become flatter and flatter and the peak intensity considerably decreases. The hole (observed for few tens of microseconds) disappears. Figure 5 shows an image

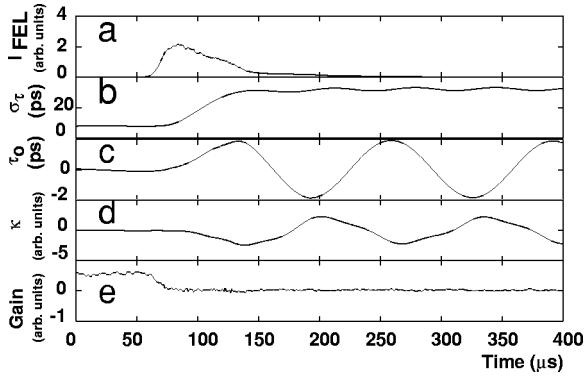

FIG. 1. Simulations using the model of localized energy exchange, performed in the case of the SOLEIL FEL operated in the *Q*-switched mode. (a) FEL intensity, (b) rms value, (c) center of mass, (d) relative variation (with respect to the laser off value) of the third order momentum of the temporal distribution versus time, and (e) FEL gain versus time.

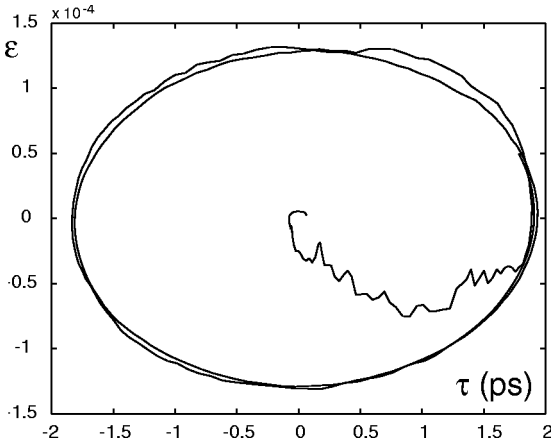

FIG. 2. Enhancement of the oscillations of barycenters of the beam longitudinal distributions due to the interaction with the FEL pulse.

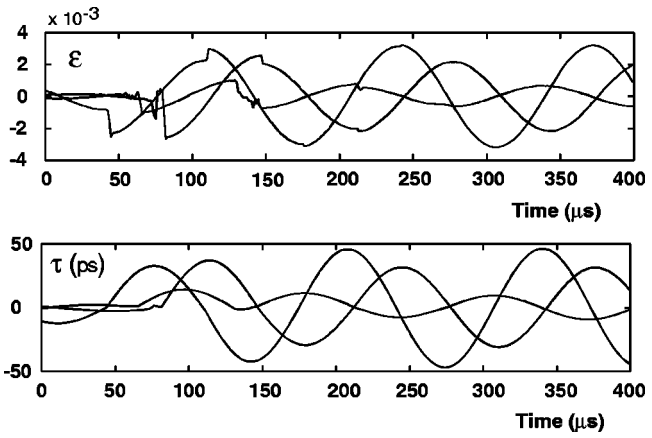

FIG. 3. Phase coordinates of three electrons inside the electron bunch during the laser evolution for the case of the SOLEIL FEL.

(equivalent to the ones that can be registered by making use of a double sweep streak camera [36–38]) that clearly emphasizes the presence of the hole burning at the center of the temporal distribution. The electron diffusion time is long compared to the revolution frequency (hundreds of nanoseconds), the period of the synchrotron oscillation (tens of microseconds), the FEL rising time (several microseconds). The diffusion time is nevertheless smaller than the natural FEL period (few milliseconds) and the synchrotron damping time (tens of milliseconds). At the end of the macropulse the diffusion process leads the longitudinal distributions back to their original Gaussian shape.

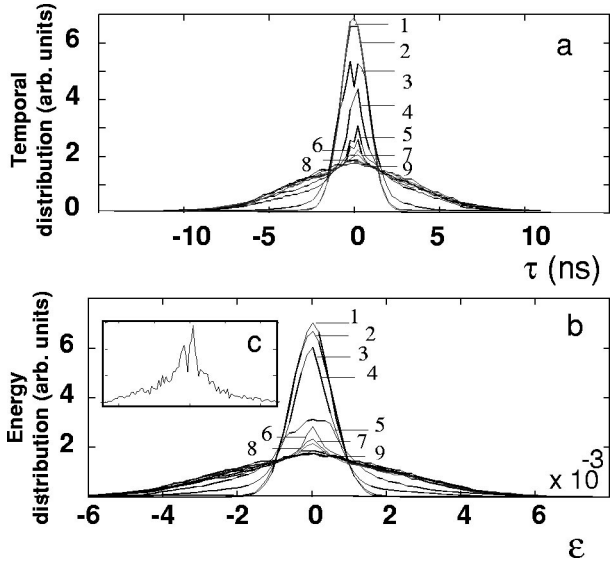

FIG. 4. Profiles of the electron longitudinal distributions for SOLEIL at different times of the dynamic evolution (average of 36 μs). curve *a*: evolution during the first 36 μs; curve *b*: evolution during 36–72 μs; curve *c*: evolution during 72–108 μs; curve *d*: evolution during 108–144 μs; curves *e, f, g, h, i*: evolution during the following 180 μs. (a) Temporal distribution (b) Energy distribution and (c) Hole burning in the energy distribution for the electrons located at $t=0$, in coincidence with the FEL pulse.

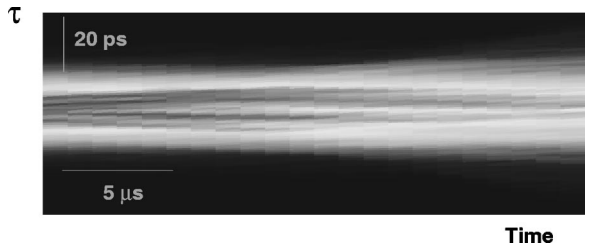

FIG. 5. Simulation of the image that can be acquired by means of a double-sweep streak camera. The aim is the characterization of the evolution of the temporal beam distribution during the laser growth for the case of the SOLEIL FEL. A cut along the vertical axes provides the longitudinal beam distribution whose evolution can be followed versus time on the horizontal scale.

B. Expected action on other storage ring FELs

The distortion of the electron bunch distributions can be generally related to the ratio between the FEL macropulse rise time τ and the synchrotron oscillations period T_s. For a generic laser system characterized by a gain G and subject to the losses P, is given by the relation

$$\tau = \frac{T_c}{(G-P)}, \tag{3}$$

where T_c is the period of the photons inside the cavity.

For small values of $r=\tau/T_s$ the electrons can be considered as quasistatic during the growth of the FEL macropulse. As a consequence, the phase-space refreshing is modest and the localized character of the interaction is exalted. In this case a distortion localized around the center of the beam distributions (where the FEL rise takes place) is generally evident. To the contrary, if r is relatively large, the FEL action during the growth of the macropulse is experimented by a large number of electrons and generally the beam distributions are heated and flattened but less locally distorted.

One of the beam optics parameter controlling the factor r is the momentum compaction α: when α is small, the longitudinal position of electrons changes slowly [see Eq. (1)] while for big values of such parameter the synchrotron period (proportional to $1/\sqrt{\alpha}$) becomes shorter and the electrons move faster. The values of r and the effect of the interaction (estimated making use of the model presented in Sec. II) on the longitudinal beam distributions for different storage-ring FELs is reported in Table II. The local distortion of beam distributions is generally more evident for third generation storage-ring FELs, as SOLEIL (see preceding section) or ELETTRA, which are characterized by small values of α and short FEL rise times. The cases of FELs installed on second generation storage rings (as Super-ACO, DUKE, and UVSOR) can be considered as intermediate: simulations show both a moderate localized distortion of the longitudinal distributions and an important flattening. In the case of the ACO FEL (installed on a first generation storage ring) the effect of the interaction on the beam distributions is very widespread (big r value).

The particular kind of distortion induced by the FEL action on the beam distributions (local distortion, flattening or

TABLE II. Action of the localized laser-beam interaction on longitudinal electron distributions for different storage ring FELs. For the calculation of the parameter $r=\tau/T_s$, the macro-pulse rise-time τ has been derived according to the relation (3) for all storage ring FELs except for the Super-ACO one (for which the experimental value has been used).

SR	α	r	Result of the interaction
SOLEIL	6.9×10^{-3}	0.004	Strong localized distortion
ELETTRA	6.9×10^{-3}	0.007	Strong localized distortion
DUKE	8.6×10^{-2}	0.1	Localized distortion and flattening
UVSOR	8.6×10^{-2}	0.15	Localized distortion and flattening
Super-ACO	1.4×10^{-2}	0.4	Localized distortion and flattening
ACO	8.6×10^{-2}	3.6	Strong flattening

both) plays an important role in the determination of the laser performances. In fact, the coupling between laser and beam energy spread takes place not only through their intensity, but also through the shape of their distributions. The form function of the electron and laser distributions are determined by second order equations that lead to a variety of solutions, including deterministic chaos, limit cycle, and steady state solutions that are of interest for user applications. Moreover, the modification of the electronic density can originate a change of the FEL pulse shape: substructures have been observed both in the spectral line and in the temporal distribution on different storage-ring FELs [30,39].

C. Measurements versus simulations for the Super-ACO and the ACO FELs

Measurements have been performed on the Super-ACO and ACO FELs in order to check the theoretical results. In the first case, use has been made of a double sweep camera that allows one to follow the electron bunch temporal distribution along the FEL macropulse evolution. The measurements (resp. simulations) of FEL pulse and the momenta of the temporal beam distribution (up to third order) are plotted in Figs. 6 curves $(a$–$d)$ [resp. Figs. 6 curves $(e$–$h)$]. The center of mass of the electronic distribution is displaced because of the energy loss due to the FEL power. In addition to the well known FEL heating, the distribution presents some oscillations, demonstrating that the dynamics is more complex than a simple bunch lengthening and enhancement of energy spread. The third order momentum κ shows the effect of the localized heating, inducing a modification of the electron bunch shape. The initial distribution is already asymmetrical $(\kappa\neq0)$ because of the microwave instability. The good agreement between experimental data and simulations strongly depends on the inclusion in the numerical model of the interaction of the electron beam with the ring environment. In particular, the same set of simulations performed without including the term $r(\tau_n)$ in Eq. (2) does not properly reproduce neither the anomalous (FEL off) bunch lengthening, nor the evolution of the third order momentum κ.

The influence of the localized FEL heating on the shape of the electronic density has been further investigated considering the case of the ACO FEL [40] operated in cw regime. In this case a flattening of the longitudinal electron bunch distributions is particularly evident (see Table II). The measured ACO temporal distribution [Fig. 7(a)] shows a shape similar to the simulated one [Fig. 7(b)]. The modification of the energy distribution is shown in Fig. 7(c).

IV. LOCAL EVOLUTION OF THE FEL-BEAM SYSTEM PARAMETERS

In the preceding section the localized character of the FEL-beam interaction has been theoretically and experimentally analyzed. In the present one, it will be shown that the concept of localized interaction leads to a definition of the system parameters involving only those electrons which superimpose with the FEL pulse. The case of the Super-ACO FEL will be considered.

Figure 8 shows the behavior of the electronic density ρ_e

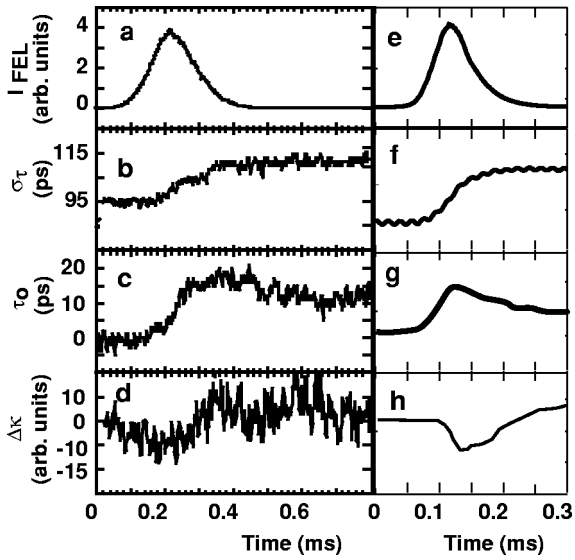

FIG. 6. Evolution of the longitudinal profile of the electronic distribution on the Super-ACO FEL operated in the Q-switched mode. Curves (a), (b), (c), and (d): experimental results; curves (e), (f), (g), (h): numerical results. The gain is established during 2 ms and suppressed during 98 ms by a modification of the tuning condition (large change of the rf frequency). The Super-ACO electron beam is operated with a current ranging between 100 and 25 mA in two bunches and with two rf cavities: $V_{\mathrm{rf1}}=170$ KV, $\omega_{\mathrm{rf1}}=100$ MHz and $V_{\mathrm{rf2}}=90$ KV, $\omega_{\mathrm{rf2}}=500$ MHz; $\alpha=1.48\times10^{-2}$. The effect due to presence of a further cavity has been taken into account in the simulations.

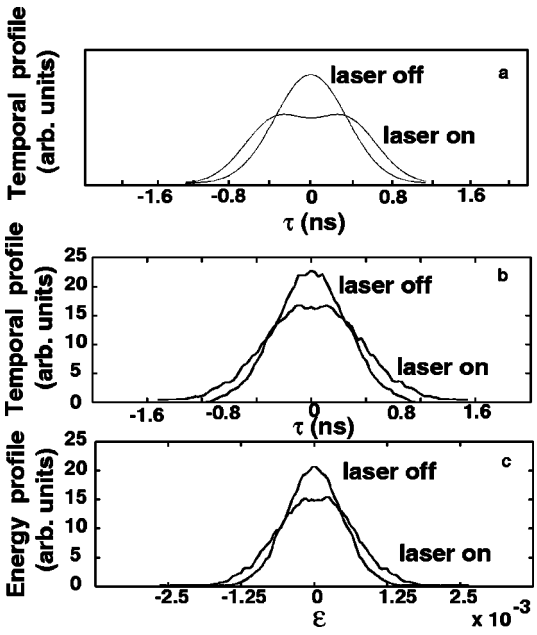

FIG. 7. Measurement and simulations for the ACO FEL being operated at 220 MeV, with a rf voltage of 17.5 kV, an average current varying from 20 to 150 mA, allowing a gain of 0.3%; curve (*a*): Measured temporal distribution with the FEL on and off. The electron bunch distribution has been deduced from the spectrum analyzer acquisition from the signal of a pick-up electrode; (*b*): Simulated temporal distribution (average of 80 μs); (*c*) Simulated energy distribution (average of 80 μs).

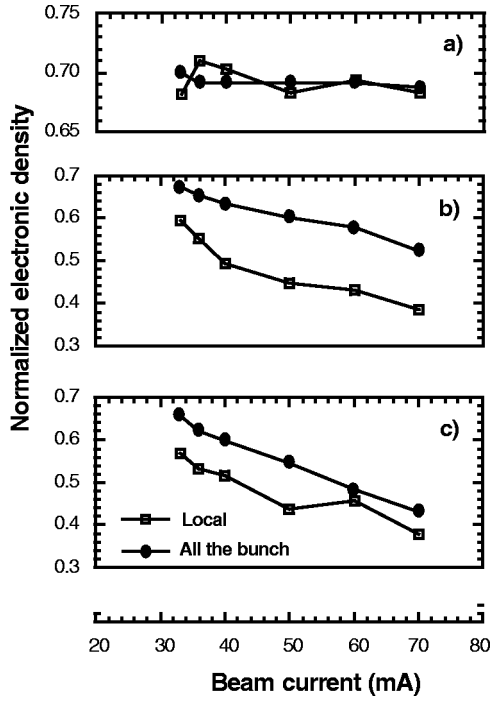

FIG. 8. Local and nonlocal Super-ACO electronic density as a function of the beam current calculated before the laser starting (a), at the top (b), and at the end of the laser pulse (c).

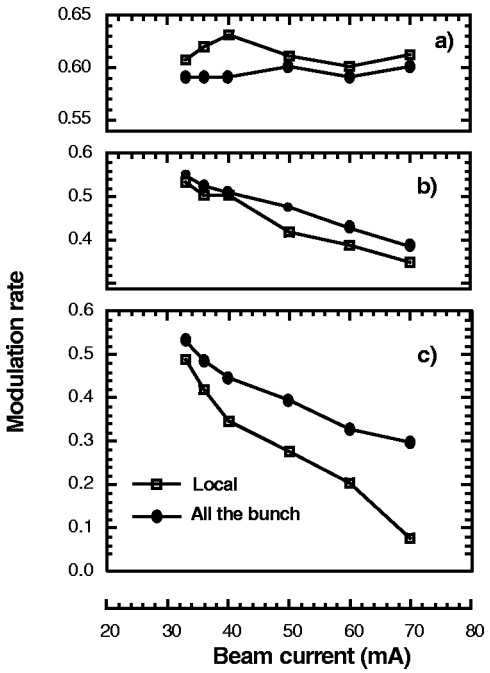

FIG. 9. Local and nonlocal modulation rate of the spectrum of the Super-ACO optical klystron as a function of the beam current calculated before the laser starting (a), at the top (b), and at the end of the laser pulse (c).

as a function of the beam current for two different cases: when the calculation is extended to all the electrons belonging to the bunch and when only those electrons interacting with the laser pulse are taken into account. The two calculations are compared at different stages of the laser growth: they are very close before the laser start [see Fig. 8(a)] but at the top and at the end of the laser pulse [see Figs. 8(b) and 8(c)] the local electronic density is considerably smaller than the one calculated on the all bunch.

The same kind of analysis has been performed for the modulation rate *f*, which is defined by the relation

$$f=\langle\cos[(N+N_d)\epsilon]\rangle. \tag{4}$$

Figure 9 shows the difference between the calculation done as an average on the electrons of the whole bunch or as a local average on the electrons that overlap the FEL pulse. Again, the local calculation performed at different stages of the FEL evolution generally leads to smaller values with respect to the nonlocal one.

The calculation of the local electronic density and modulation rate can be used to draw out the effective (local) FEL gain G (which is proportional to $\rho_e f$). Figure 10 shows the calculation of the FEL gain either according to the standard nonlocalized approach or considering only the electrons seen by the laser during its growth. When the laser is absent the two methods give the same result [see Fig. 10(a)] but at the top of the laser macropulse (where, for definition, the gain must be equal to the cavity losses) only the local gain curve explains the saturation effect [see Fig. 10(b)].

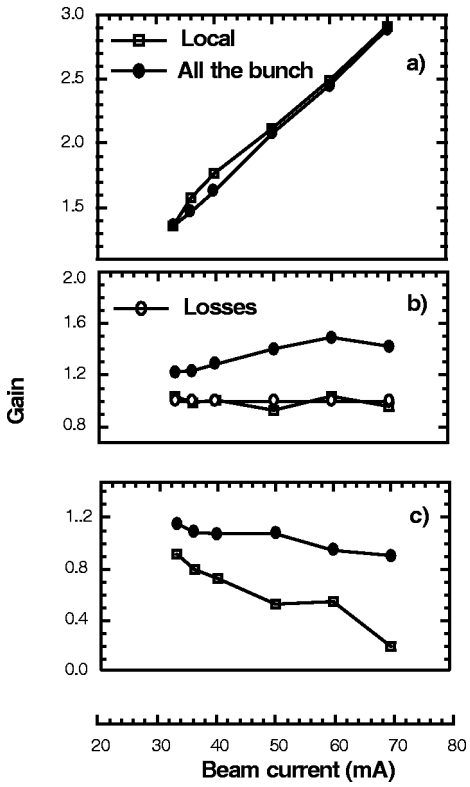

FIG. 10. Local and nonlocal Super-ACO FEL gain as a function of the beam current calculated before the laser starting (a), at the top of the laser pulse (b), and at the end of the laser pulse (c). Figure (b) shows also the value of the cavity losses.

The localized character of the FEL-beam interaction is therefore crucial for explaining the laser saturation for the case of the Super-ACO FEL.

The reduction of the effective gain can in part explain the important difference that has been observed between the theoretical and the measured values of the rise time for the Super-ACO FEL operated in *Q*-switched regime. Experimentally τ can be determined by means of an exponential fit

$$I(t) = I_0 \exp\left(\frac{t}{\tau}\right) \tag{5}$$

(where I_0 is the initial laser intensity) of the first part of the laser pulse curve.

If the localized character of the interaction is not taken into account, the difference between the theoretical value and the measured one is quite significant (of the order of 30% between 30 and 40 mA and up to 50% for higher currents). To the contrary, when the gain is instead calculated using the local parameters, the result obtained using Eq. (3) is more close to the measured value (the difference being about 10% between 30 and 40 mA and less than 30% for higher currents).

V. CONCLUSIONS

The analysis presented in this paper provides an additional step further in the understanding of the interaction between light and relativistic electrons. We presented a pass to pass model of the electron dynamics in the longitudinal phase-space based on the local interaction with a short laser pulse. On condition that the important role of the wake fields is taken into account, such a model can be successfully applied for describing the laser-beam interaction in a storage-ring FEL. Simulations are indeed supported by experimental results on the Super-ACO and the ACO FELs.

The type of distortion induced by the interaction on the beam longitudinal distributions has been correlated to a quality factor depending on the beam and laser dynamics. Such a distortion is expected to influence the FEL form function. The redefinition of the system parameters by taking into account only those electrons that overlap with the laser pulse is the only way to explain the saturation of the Super-ACO FEL.

The proposed model applies not only to storage-ring FELs operated both in *Q*-switched and cw regimes but also to the study of the interaction of the electron beam with an external laser. This approach is able to provide important insights in view of the development of new generation synchrotron radiation facilities that can include, besides FELs, various exotic light sources such as femtosecond x-ray pulses and Compton back scattering gamma rays.

[1] F. Glotin *et al.*, Phys. Rev. Lett. **77**, 3130 (1996).
[2] A. A. Zholents *et al.*, Phys. Rev. Lett. **76**, 1652 (1983).
[3] A. Esarey *et al.*, IEEE Trans. Plasma Sci. **24**, 252 (1996).
[4] D. A. G. Deacon *et al.*, Phys. Rev. Lett. **38**, 892 (1977).
[5] M. Billardon *et al.*, Phys. Rev. Lett. **51**, 1652 (1983).
[6] V. Litvinenko *et al.* (unpublished).
[7] R. Prazeres *et al.*, IEEE J. Quantum Electron. **27**, 1061 (1991).
[8] A. Renieri, Nucl. Instrum. Methods Phys. Res. A **375**, 1 (1996).
[9] G. Dattoli *et al.*, Phys. Rev. E **58**, 6570 (1998).
[10] M. Migliorati and L. Palumbo, Riv. Nuovo Cimento **112**, 461 (1999).
[11] H. Hama, J. Yamazaki, and G. Isoyama, Nucl. Instrum. Methods Phys. Res. A **341**, 12 (1994).
[12] M. E. Couprie *et al.*, Nucl. Instrum. Methods Phys. Res. A **304**, 58 (1991).
[13] H. Hama and M. Hosaka, Nucl. Instrum. Methods Phys. Res. A **429**, 172 (1999).
[14] M. E. Couprie *et al.*, Nucl. Instrum. Methods Phys. Res. A **358**, 374 (1995).
[15] M. E. Couprie *et al.*, Rev. Sci. Instrum. **65**, 1485 (1994).
[16] M. Marsi *et al.*, Appl. Phys. Lett. **70**, 895 (1997).
[17] R. P. Walker *et al.*, Nucl. Instrum. Methods Phys. Res. A **429**, 179 (1999).
[18] M. E. Couprie *et al.*, Nucl. Instrum. Methods Phys. Res. B **144**, 66 (1988).

[19] A. Renieri, Riv. Nuovo Cimento **53B**, 161 (1979).
[20] G. Dattoli and A. Renieri, Riv. Nuovo Cimento **59B**, 1 (1980).
[21] G. Dattoli *et al.*, Phys. Rev. A **37**, 4326 (1988).
[22] V. N. Litvinenko *et al.*, Nucl. Instrum. Methods Phys. Res. A **358**, 369 (1995).
[23] V. N. Litvinenko *et al.*, Nucl. Instrum. Methods Phys. Res. A **375**, 46 (1996).
[24] K. Oide *et al.*, KEK Report 90-10, 1990 (unpublished).
[25] G. V. Stupakov *et al.*, Phys. Rev. E **55**, 5976 (1997).
[26] G. Dattoli *et al.*, Nuovo Cimento Soc. Ital. Fis., A **112A**, 491 (1999).
[27] A. Mosnier, Nucl. Instrum. Methods Phys. Res. A **438**, 225 (1999).
[28] M. Billardon, Phys. Rev. Lett. **65**, 713 (1990).
[29] M. E. Couprie *et al.*, Nucl. Instrum. Methods Phys. Res. A **318**, 59 (1992).
[30] H. Hama *et al.*, Nucl. Instrum. Methods Phys. Res. A **375**, 32 (1996).
[31] N.A. Vinokurov *et al.* (unpublished).
[32] R. Roux, M. Billardon, Nuovo Cimento Soc. Ital. Fis., A **112**, 513 (1999).
[33] P. Elleaume, J. Phys. Colloq. **44**, 333 (1983).
[34] M. Sands, SLAC Report No. 121, 1970 (unpublished).
[35] T. Hara *et al.*, Nucl. Instrum. Methods Phys. Res. A **A375**, 39 (1996).
[36] R. Roux *et al.*, Nucl. Instrum. Methods Phys. Res. A **393**, 33 (1997).
[37] H. Hama *et al.*, Nucl. Instrum. Methods Phys. Res. A **358**, 365 (1995).
[38] A. H. Lumpkin, B. X. Yang, and Y. C. Chae, Nucl. Instrum. Methods Phys. Res. A **393**, 50 (1997).
[39] M. E. Couprie *et al.*, Phys. Rev. E **53**, 1871 (1996).
[40] M. Billardon *et al.*, Phys. Rev. Lett. **51**, 1652 (1983).